Received: 28 June 2019 | Revised: 7 March 2020 | Accepted: 3 June 2020

DOI: 10.1002/rnc.5120

RESEARCH ARTICLE

WILEY

A complementary quantitative feedback theory solution to the 2 × 2 tracking error problem

Arnold Pretorius | **Edward Boje**

Department of Electrical Engineering, University of Cape Town, Cape Town, South Africa

Correspondence
Arnold Pretorius, Department of Electrical Engineering, University of Cape Town, Cape Town, Western Cape, 7700, South Africa.
Email: prtarn001@myuct.ac.za

Funding information
South African Agency for Science and Technology Advancement, Grant/Award Number: 81148

Summary

This article presents a solution to the 2 × 2 multivariable tracking error problem. Current quantitative feedback theory methods commonly employ plant-inverting splittings in order to arrive at an approximately decoupled design on the feedback control elements. This results in suitable design regions in the high-gain, low-frequency range, but can result in conservative design at and above the gain-crossover frequency, resulting in overdesigned feedback controllers. Our method aims to reduce this conservatism by supplementing a plant-inverting design with a non-plant-inverting design, which tends to perform well at higher frequencies. Decoupling the design of the controller elements is facilitated by making use of appropriate existence conditions. The union of the two resulting design regions then describes a larger solution space, and by enlarging the admissible design regions for the feedback controller, lower gain feedback controller design at all design frequencies of interest may be possible. A benchmarking example is presented, showing the viability of the proposed method.

KEYWORDS

MIMO QFT, robust control, tracking error specifications

1 | INTRODUCTION

In terms of the single-input-single-output (SISO) QFT tracking problem, nonconservative (ie, exact) solutions exist, be it in the form of above/below tracking magnitude bounds,[1] or tracking error bounds[2,3] However, in the case of solving multi-input-multi-output (MIMO) problems, the current state of the art involves varying levels of conservatism.[4] This comes as a result of two design challenges, namely, (i) the bandwidth trade-off between feedback controller and prefilter and (ii) decoupling the design of the feedback control elements. (i) was originally addressed by using the method of above/below magnitude specifications on the reference to output transfer behavior.[5] The structure of the design equations however requires the use of a diagonal prefilter, which may artificially limit the potential gain saving in the feedback controller. Additionally, the lack of phase information present in the specifications incurs additional conservatism, and can reduce tracking precision.[6] The concept of bounding the reference model tracking error was introduced for SISO systems in Reference 7. This method handles the two-degree-of-freedom (2DOF) trade-off by setting the prefilter equal to the prescribed model performance, prior to design of the feedback controller. This simple method captures phase information between the model and closed-loop response, and allows for direct design on the feedback controller. The suboptimal

Abbreviations: QFT, quantitative feedback theory; SISO, single-input-single-output; MIMO, multi-input multi-output; 2DOF, two-degree-of-freedom.
Arnold Pretorius and Edward Boje contributed equally authors.

selection of the prefilter however places unnecessary overdesign on the feedback controller. The multivariable equivalent method was developed in Reference 8, whereby the nominal prefilter additionally incorporates information from a selected nominal plant . Once the feedback controller has been designed, the prefilter is adjusted (if need be) by inferring differential error specifications on the nominal prefilter. Although this assists the bandwidth trade-off, selection of an appropriate nominal plant for the entire frequency range of interest is not obvious, and may lead to additional overdesign on the feedback control design. A different design methodology was introduced in Reference 9, whereby a sensitivity design could proceed, based on establishing necessary conditions for meeting the tracking error specifications. A diagonal prefilter could then be designed subsequently, using the original tracking error specifications. This method has the benefit that the feedback control design is not biased by a selected nominal plant. The aforementioned necessary conditions however do not guarantee that the design can be completed. More recently, a less conservative solution was proposed, which separates the elementwise tracking error problem into a simultaneous tracking and disturbance rejection problem, using manual bound balancing methods.[10] The design of the prefilter and feedback controller can then be decoupled, by defining existence conditions on the elementwise prefilter solution space. Successful design of the diagonal feedback controller enables the design of a fully populated prefilter. This method is similarly implemented for the measured disturbance rejection problem in Reference 11. However, as an optimal bound balancing requires the scaling parameter to vary with the controller phase and particular plant instance (to ensure both design regions overlap perfectly), the implementation in Reference 10 will, in general, incur additional design conservatism.

Although the aforementioned methods handle the 2DOF bandwidth trade-off of (i) with varying success, the feedback controller decoupling of (ii) is, in general, facilitated by using plant-inverting splittings. The natural drawback of this splitting is the required feedback design conservatism at higher frequencies where low loop gain is desired, as a result of the (potentially) improper plant inverse rolling up at high frequency. As the designer is primarily concerned with feedback design in the gain-phase crossover region, one can only benefit from having more design freedom at the higher frequencies, especially in the case of nonminimum phase systems. This article therefore presents a novel method, geared at 2×2 plants, which combines a plant-inverting design routine with a non-plant-inverting design. First, the bandwidth trade-off is facilitated by defining appropriate existence conditions for a feedforward filter, which can meet the tracking specifications. The plant-inverting method is then used to generate acceptable design regions for the feedback controller, which generally incur less design conservatism at low frequencies. Similarly, using a non-plant-inverting method, one can arrive at design regions on the feedback controller, which are less conservative at high frequencies. As only one of the two resulting design regions needs to be adhered to, the union of the two regions describes an expanded solution space, on a discrete frequency-by-frequency basis. In this way, the designer has more freedom in shaping the feedback controller behavior. Once the feedback control design is complete, the nondiagonal prefilter is designed without the use of overbounding methods, using similar existence conditions for meeting the underlying tracking error specifications. As this method is a QFT design tool, which finds feasible regions at discrete design frequency points, the designer is still required to join these regions with a low order, causal controller, capable of achieving closed-loop plant stability. This method is benchmarked using a simple example, which demonstrates its utility, especially at the higher frequencies.

2 | PROBLEM STATEMENT

Consider the two 2DOF control configurations of Figures 1 and 2, where $P^i(s)$ is a 2×2 plant instance in the uncertain set $\mathcal{P}(s)$, $r(s)$ is the 2×1 reference signal, and $M(s)$ is the 2×2 reference model to be tracked. The set $\mathcal{P}(s) = \{P^1(s), P^2(s), \dots, P^n(s)\}$ is an ε-*net* of disjoint plants, which sufficiently describes the uncertain plant. Diagonal feedback controller $G(s)$=diag$\{g_1(s),g_2(s)\}$ acts to reduce uncertainty across the plant set, while 2×2 prefilter $F(s)$ (feedforward filter $X(s)$ in Figure 2) is designed to adjust the closed-loop bandwidth of the plant set, as required.

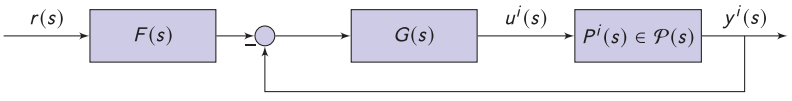

FIGURE 1 Block diagram of conventional control configurations with two degrees of freedom, $\{G(s), F(s)\}$ [Colour figure can be viewed at wileyonlinelibrary.com]

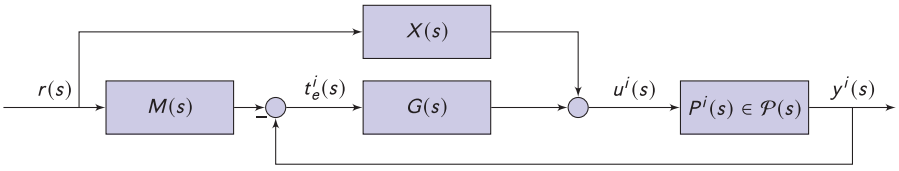

FIGURE 2 Block diagram of feedforward control scheme (still with two degrees of freedom, $\{G(s), X(s)\}$) [Colour figure can be viewed at wileyonlinelibrary.com]

If $F(s) = M(s) + G^{-1}(s)X(s)$, both schemes are equivalent. The structure in Figure 2 however has the benefit in that it inherently captures the reference model tracking error

$$t_e^i(s) = E^i(s)r(s) = M(s)r(s) - y^i(s), \tag{1}$$

where

$$E^i(s) = (I + P^i(s)G(s))^{-1}(M(s) - P^i(s)X(s)). \tag{2}$$

Following standard tracking error QFT methods,[8] the elementwise magnitude of the matrix reference model tracking error frequency response in (2) can be constrained by a defined specification,

$$|e_{rc}^i(j\omega_d)| \leq \beta_{rc}(\omega_d), \tag{3}$$

where $\beta_{rc}(\omega_d)$ is the user-specified reference model tracking error tolerance at row r and column c, and $\omega_d \in \Omega$ is the discrete design frequency point of interest. The design frequency set, Ω, is chosen based on engineering understanding of the control problem, and is required to be sufficiently rich, in order to capture the contiguous frequency behavior of the closed-loop system. The objective is to design $G(s)$ and $X(s)$ in order to meet the constraints of (3) for all plant cases, $i \in \{1,2,\dots,n\}$. Additionally, cost-effective design requires that the bandwidth and complexity/order of $G(s)$ be minimized.

3 | METHOD

3.1 | Feedback control design

3.1.1 | Plant-inverting splitting

The relationship between $X(j\omega_d)$ and $G(j\omega_d)$ can be assessed by using diagonal matrix splittings. This is commonly used to decouple the elementwise design of $G(s)$, at the cost of coupling the elements of $E^i(s)$. With reference to (2), premultiplying both sides by $(\hat{P}^i(s) + G(s))$, where $\hat{P}^i(s)$ is the inverse of $P^i(s)$,

$$(\hat{P}^i(s) + G(s))E^i(s) = \hat{P}^i(s)M(s) - X(s). \tag{4}$$

Next, splitting $\hat{P}^i(s)$ into its diagonal and off-diagonal components, $\hat{P}^i(s) = \hat{P}_d^i(s) + \hat{P}_n^i(s)$, (4) can be written as

$$(\hat{P}_d^i(s) + G(s))(I + (\hat{P}_d^i(s) + G(s))^{-1}\hat{P}_n^i(s))E^i(s) = \hat{P}^i(s)M(s) - X(s). \tag{5}$$

Finally, $E^i(s)$ can be written implicitly, thereby becoming decoupled with respect to design variable $G(s)$,

$$E^i(s) = (\hat{P}_d^i(s) + G(s))^{-1}(\hat{P}^i(s)M(s) - X(s) - \hat{P}_n^i(s)E^i(s)). \tag{6}$$

Making use of (3), the elementwise magnitude constraints of (6) for a 2×2 problem, evaluated at discrete design frequency point ω_d, follows as

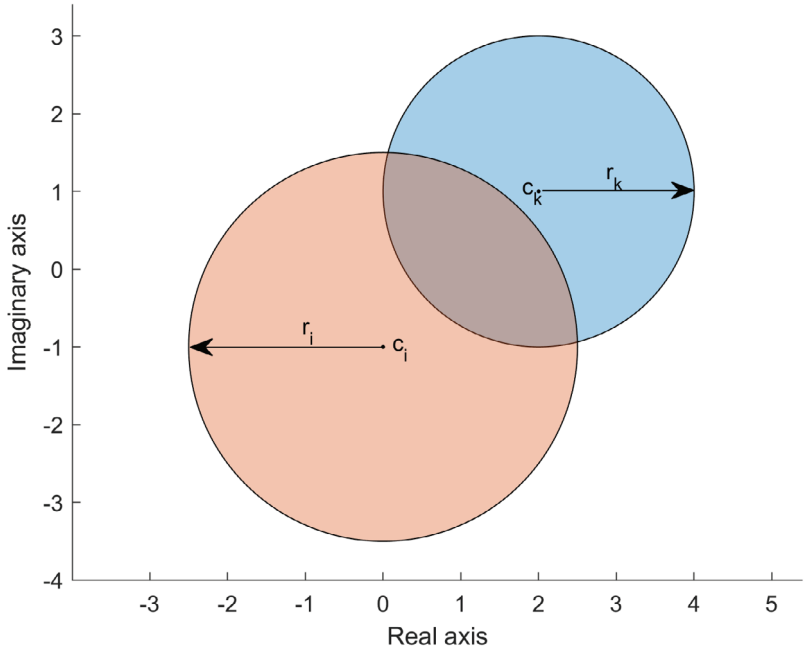

FIGURE 3 Arithmetic-complex plane of $x_{rc}(j\omega_d)$ showing nonempty intersection of two discoidal design regions. Overlapping occurs when $|c_i - c_k| \leq r_i + r_k$. A valid $x_{rc}(j\omega_d)$, which simultaneously satisfies plant instance i and k, is required to lie within the area of intersection [Colour figure can be viewed at wileyonlinelibrary.com]

$$\begin{bmatrix} |e_{11}| & |e_{12}| \\ |e_{21}| & |e_{22}| \end{bmatrix}^i_{\omega_d} = \begin{bmatrix} \frac{|(\hat{p}_{11}m_{11} + \hat{p}_{12}m_{21} - x_{11}) - \hat{p}_{12}e_{21}|}{|\hat{p}_{11} + g_1|} & \frac{|(\hat{p}_{11}m_{12} + \hat{p}_{12}m_{22} - x_{12}) - \hat{p}_{12}e_{22}|}{|\hat{p}_{11} + g_1|} \\ \frac{|(\hat{p}_{21}m_{11} + \hat{p}_{22}m_{21} - x_{21}) - \hat{p}_{21}e_{11}|}{|\hat{p}_{22} + g_2|} & \frac{|(\hat{p}_{21}m_{12} + \hat{p}_{22}m_{22} - x_{22}) - \hat{p}_{21}e_{12}|}{|\hat{p}_{22} + g_2|} \end{bmatrix}^i_{\omega_d} \leq \begin{bmatrix} \beta_{11} & \beta_{12} \\ \beta_{21} & \beta_{22} \end{bmatrix}_{\omega_d}. \tag{7}$$

The unknown $e^i_{rc}(j\omega_d)$ terms appearing implicitly in (7) necessitates an overbounding, using the triangle inequality, which results in the conservative elementwise constraint[8] of

$$\begin{bmatrix} |e_{11}| & |e_{12}| \\ |e_{21}| & |e_{22}| \end{bmatrix}^i_{\omega_d} \leq \begin{bmatrix} \frac{|\hat{p}_{11}m_{11} + \hat{p}_{12}m_{21} - x_{11}| + |\hat{p}_{12}|\beta_{21}}{|\hat{p}_{11} + g_1|} & \frac{|\hat{p}_{11}m_{12} + \hat{p}_{12}m_{22} - x_{12}| + |\hat{p}_{12}|\beta_{22}}{|\hat{p}_{11} + g_1|} \\ \frac{|\hat{p}_{21}m_{11} + \hat{p}_{22}m_{21} - x_{21}| + |\hat{p}_{21}|\beta_{11}}{|\hat{p}_{22} + g_2|} & \frac{|\hat{p}_{21}m_{12} + \hat{p}_{22}m_{22} - x_{22}| + |\hat{p}_{21}|\beta_{12}}{|\hat{p}_{22} + g_2|} \end{bmatrix}^i_{\omega_d} \leq \begin{bmatrix} \beta_{11} & \beta_{12} \\ \beta_{21} & \beta_{22} \end{bmatrix}_{\omega_d}. \tag{8}$$

Multiplying through by the elementwise denominator of (8), the generalized conservative constraint for $|e^i_{rc}(j\omega_d)|$ is

$$|\hat{p}_{r1}m_{1c} + \hat{p}_{r2}m_{2c} - x_{rc}|^i_{\omega_d} \leq |\hat{p}_{rr} + g_r|\beta_{rc}|^i_{\omega_d} - |\hat{p}_{rv}|\beta_{vc}|^i_{\omega_d}, \tag{9}$$

where $v = (2, 1)$ for $r = (1, 2)$, respectively. The amount of conservatism induced by overbounding in (8) is related to the size of $|\hat{p}_{rv}|\beta_{vc}|^i_{\omega_d}$, relative to the size of $\beta_{rc}|\hat{p}_{rr} + g_r||^i_{\omega_d}$. In particular, if $|\hat{p}_{rv}|\beta_{vc}|^i_{\omega_d} << \beta_{rc}|\hat{p}_{rr} + g_r||^i_{\omega_d}$, there will be negligible conservatism. For the class of problems with zero steady-state tracking error specifications, $P^i(s)$ and/or $G(s)$ will contain at least one integrator in the channel of interest. This means that $\beta_{rc}|\hat{p}_{rr} + g_r||^i_{\omega_d}$ will dominate $|\hat{p}_{rv}|\beta_{vc}|^i_{\omega_d}$ at low frequencies (implying low design conservatism), whereas the opposite will occur at high frequencies for sufficiently coupled plants (implying high design conservatism). This is a natural result of the plant-inverting splitting.[4] With reference to Figure 3, (9) can be written as

$$|c_i - x_{rc}(j\omega_d)| \leq r_i, \tag{10}$$

and geometrically describes the discoidal solution space of $x_{rc}(j\omega_d)$ (for plant instance i), with center $c_i = (\hat{p}_{r1}m_{1c} + \hat{p}_{r2}m_{2c})|^i_{\omega_d}$, and radius $r_i = (\beta_{rc}|\hat{p}_{rr} + g_r| - |\hat{p}_{rv}|\beta_{vc})|^i_{\omega_d}$.

Note that the radius of the admissible design region is reduced by the worst-case phase of $-\hat{p}_{rv}e_{vc}|^i_{\omega_d}$. In order for a $x_{rc}(j\omega_d)$ to exist which satisfies (9) for all plant cases, there must be a common intersection for the set of plant dependent discoidal design regions. This necessitates that the distance between each ordered (by plant index) pair of disc centers must be smaller than or equal to the sum of their respective radii ($|c_i - c_k| \leq r_i + r_k$),[3]

$$|(\hat{p}^i_{r1} - \hat{p}^k_{r1})m_{c1} + (\hat{p}^i_{r2} - \hat{p}^k_{r2})m_{c2}|_{\omega_d} \leq \beta_{rc}(\omega_d(|\hat{p}_{rr} + g_r|^i_{\omega_d} + |\hat{p}_{rr} + g_r|^k_{\omega_d}) - \beta_{vc}(\omega_d)(|\hat{p}_{rv}|^i_{\omega_d} + |\hat{p}_{rv}|^k_{\omega_d}), \quad \forall i, k. \tag{11}$$

Ensuring that each ordered pair of discs individually intersect, does not, in general, guarantee that a common intersection exists across all discs (contrary to the affirmation originally stated in Reference 3). However, the likelihood of a common intersection occurring will increase as the number of discs increase (each disc's radius is parameterized by a common $g_r(j\omega_d)$). Eq. 11 is solely a function of $g_r(j\omega_d)$ and can be used to generate design regions directly on $g_r(j\omega_d)$. Interestingly, the per-plant solution space of $g_r(j\omega)$ is a "stay-out" ellipse, with foci at $-\hat{p}^i_{rr}(j\omega_d)$ and $-\hat{p}^k_{rr}(j\omega_d)$, and a major axis of $(|(\hat{p}^i_{r1} - \hat{p}^k_{r1})m_{c1} + (\hat{p}^i_{r2} - \hat{p}^k_{r2})m_{c2}| + \beta_{vc}(|\hat{p}_{rv}|^i + |\hat{p}_{rv}|^k))/\beta_{rc}|_{\omega_d}$. This closely resembles the result in Reference 3. For a 2×2 plant, there will be two sets of constraints for the particular $g_r(j\omega_d)$ because two elements in (8) depend on $g_r(j\omega_d)$. It is worth noting that the design regions on $g_r(j\omega_d)$, resulting from (11), would be equivalent to that of[10] if the scaling parameters used in the bound balancing stage of[10] were selected optimally for the particular plant instance (as the "worst-case" plant may vary across the partitioned bounds) and controller phase angle (in order to ensure that one boundary does not dominate the other boundary at any phase angle). The nonempty intersection of the resulting design regions describes the (conservative) solution space of $g_r(j\omega_d)$, for the particular plant-inverting splitting, namely $\mathbb{S}^{\hat{P}}_{g_r(j\omega_d)}$. As with other QFT methods which incorporate the triangle inequality, the tracking tolerances may need to be adjusted, in order to arrive at a design equilibrium between loops.[12] Note that this method can be generalized for MIMO systems of any order. As previously mentioned, these design regions on $g_r(j\omega_d)$ tend to be favorable at low frequencies because of high loop gain, but may perform poorly at higher frequencies (for sufficiently coupled plants). To remedy this, we seek a complementary splitting, which will perform well at high frequencies.

3.1.2 | Non-plant-inverting splitting

A non-plant-inverting splitting is applied to (2) as follows: Premultiplying both sides of (2) by $(I + P^i(s)G(s))$ yields

$$(I + P^i(s)G(s))E^i(s) = M(s) - P^i(s)X(s). \tag{12}$$

Using a diagonal splitting, $L^i(s)$ is written as $L^i(s) = P^i(s)G(s) = L^i_d(s) + L^i_n(s)$, and (12) can be expanded as

$$(I + L^i_d(s))(I + (I + L^i_d(s))^{-1}L^i_n(s))E^i(s) = M(s) - P^i(s)X(s). \tag{13}$$

Finally, error matrix $E^i(s)$ can be described implicitly as

$$E^i(s) = (I + L^i_d(s))^{-1}(M(s) - P^i(s)X(s) - L^i_n(s)E^i(s)). \tag{14}$$

The corresponding elementwise magnitude constraint for a 2×2 system, at design frequency point ω_d, follows as

$$\begin{bmatrix} |e_{11}| & |e_{12}| \\ |e_{21}| & |e_{22}| \end{bmatrix}^i_{\omega_d} = \begin{bmatrix} \left|\frac{(m_{11}-p_{12}x_{21}-p_{11}x_{11})-p_{12}g_2e_{21}}{1+p_{11}g_1}\right| & \left|\frac{(m_{12}-p_{12}x_{22}-p_{11}x_{12})-p_{12}g_2e_{22}}{1+p_{11}g_1}\right| \\ \left|\frac{(m_{21}-p_{22}x_{21}-p_{21}x_{11})-p_{21}g_1e_{11}}{1+p_{22}g_2}\right| & \left|\frac{(m_{22}-p_{22}x_{22}-p_{21}x_{12})-p_{21}g_1e_{12}}{1+p_{22}g_2}\right| \end{bmatrix}^i_{\omega_d} \leq \begin{bmatrix} \beta_{11} & \beta_{12} \\ \beta_{21} & \beta_{22} \end{bmatrix}_{\omega_d}. \tag{15}$$

Applying the triangle inequality, (15) can be overbounded (elementwise) by

$$\begin{bmatrix} |e_{11}| & |e_{12}| \\ |e_{21}| & |e_{22}| \end{bmatrix}^i_{\omega_d} \leq \begin{bmatrix} \frac{|m_{11}-p_{12}x_{21}-p_{11}x_{11}|+|p_{12}||g_2|\beta_{21}}{|1+p_{11}g_1|} & \frac{|m_{12}-p_{12}x_{22}-p_{11}x_{12}|+|p_{12}||g_2|\beta_{22}}{|1+p_{11}g_1|} \\ \frac{|m_{21}-p_{22}x_{21}-p_{21}x_{11}|+|p_{21}||g_1|\beta_{11}}{|1+p_{22}g_2|} & \frac{|m_{22}-p_{22}x_{22}-p_{21}x_{12}|+|p_{21}||g_1|\beta_{12}}{|1+p_{22}g_2|} \end{bmatrix}^i_{\omega_d} \leq \begin{bmatrix} \beta_{11} & \beta_{12} \\ \beta_{21} & \beta_{22} \end{bmatrix}_{\omega_d}. \tag{16}$$

Multiplying through by the elementwise denominator of (16), the generalized constraint for $|e^i_{rc}(j\omega_d)|$ is

$$|m_{rc} - p_{r1}x_{1c} - p_{r2}x_{2c}|^i_{\omega_d} \leq \beta_{rc}|1 + p_{rr}g_r||^i_{\omega_d} - \beta_{vc}|p_{rv}||g_v||^i_{\omega_d}. \tag{17}$$

As the elements of $L^i(s)$ are expected to be strictly proper (by correct design), $\beta_{rc}|1+p_{rr}g_r||^i_{\omega_d}$ will dominate $\beta_{vc}|p_{rv}||g_v||^i_{\omega_d}$ at sufficiently high frequencies (outside the closed-loop bandwidth), implying low design conservatism. The low frequency counterpart will however, experience conservatism (unless the plant is weakly coupled). Unlike in (9), the structure of (17) does not lend itself to closed-form existence conditions for separating the design of $G(s)$ and $X(s)$. Instead, the uncoupled design of the control elements is facilitated by selecting a frequency response of $X(j\omega_d)$ at each design point. This prototype $X(j\omega_d)$ allows for direct design on $G(s)$, after which $X(s)$ can be designed in earnest. With reference to (17), minimizing $|m_{rc}-p_{r1}x_{1c}-p_{r2}x_{2c}|^i_{\omega_d}$ will reduce the amount of feedback gain required. Specifically, $x_{11}(j\omega_d)$ and $x_{21}(j\omega_d)$ are found to minimize $|m_{11}-p_{12}x_{21}-p_{11}x_{11}|^i_{\omega_d}$ and $|m_{21}-p_{22}x_{21}-p_{21}x_{11}|^i_{\omega_d}$ simultaneously. Similarly, $x_{12}(j\omega_d)$ and $x_{22}(j\omega_d)$ are selected to minimize $|m_{12}-p_{12}x_{22}-p_{11}x_{12}|^i_{\omega_d}$ and $|m_{22}-p_{22}x_{22}-p_{21}x_{12}|^i_{\omega_d}$. As there are multiple plant instances, the optimization aims to minimize the worst-case occurrence across the enumerated plant set. The corresponding minimax problem follows as

$$\min_{x_{1c}(j\omega_d),x_{2c}(j\omega_d)\in\mathbb{C}} \max \left\{ \sum_{r=1}^{2} \frac{|m_{rc}-p_{r1}x_{1c}-p_{r2}x_{2c}|}{\beta_{rc}}\Bigg|^i_{\omega_d}, \forall i \in \{1,2,\ldots n\} \right\}, \tag{18}$$

where $\beta_{rc}(\omega_d)$, from (3), is used to weight the terms to be minimized. Given that $x_{1c}(j\omega_d)$ and $x_{2c}(j\omega_d)$ are complex numbers, the optimization routine for column c solves for four free parameters, and is computationally straightforward. This prototype selection of $X(j\omega_d)$ can be thought of as a sufficient condition for the existence of a $X(s)$, once $G(s)$ has been designed (assuming an $X(s)$ exists which can join the discrete design regions), albeit a (potentially) more limiting one than that of (11).

Using prototype $X(j\omega_d)$ from (18), generation of the non-plant-inverting feedback design regions can commence. Notably, the constraint in (17) is a function of both $g_1(j\omega_d)$ and $g_2(\omega_d)$. In order to remove the dependence on $g_2(j\omega_d)$ when designing $g_1(j\omega_d)$ first (eg), one can define necessary and sufficient conditions on $g_1(j\omega_d)$, which guarantee the existence of at least one valid $g_2(j\omega_d)$ satisfying (17) for plant i. Setting known $K^i(j\omega_d)=M(j\omega_d)-P^i(j\omega_d)X(j\omega_d)$ for sake of clarity, the constraints on $g_2(j\omega_d)$ from the first row of (16) can be written as

$$|g_2(j\omega_d)| \le \frac{\beta_{1c}|1+p_{11}g_1|-|k_{1c}|}{\beta_{2c}|p_{12}|}\Bigg|^i_{\omega_d}, \tag{19}$$

whereas the constraints on $g_2(j\omega_d)$ from the second row of (16) can be written as

$$\left|g_2-\frac{-1}{p_{22}}\right|^i_{\omega_d} \ge \frac{|k_{2c}|+\beta_{1c}|p_{21}||g_1|}{\beta_{2c}|p_{22}|}\Bigg|^i_{\omega_d}. \tag{20}$$

With reference to Figure 4, the admissible design region of $g_2(j\omega_d)$ in (19) is a "stay-in" disc, centered at the origin ($c_1=0$), with a radius of $r_1=(\beta_{1c}|1+p_{11}g_1|-|k_{1c}|)/(\beta_{2c}|p_{12}|)|^i_{\omega_d}$, whereas the design region of (20) is a "stay-out" disc, centered at $c_2=-1/p^i_{22}(j\omega_d)$, with a radius of $r_2=(|k_{2c}|+\beta_{1c}|p_{21}||g_1|)/(\beta_{2c}|p_{22}|)|^i_{\omega_d}$.

The existence of a nonempty design region of $g_2(j\omega)$, which simultaneously satisfies (19) and (20) for plant instance i and column c demands that the "stay-out" disc does not fully envelop the "stay-in" disc. Referring to Figure 4, this requires that the distance between the centers of the two discs must be greater than or equal to the radius of the "stay-out" disc, minus the radius of the "stay-in" disc ($|c_2-c_1|\ge r_2-r_1$), explicitly described as

$$\left|\frac{1}{p_{22}}\right|^i_{\omega_d} \ge \frac{|k_{2c}|+\beta_{1c}|p_{21}||g_1|}{\beta_{2c}|p_{22}|}\Bigg|^i_{\omega_d} - \frac{\beta_{1c}|1+p_{11}g_1|-|k_{1c}|}{\beta_{2c}|p_{12}|}\Bigg|^i_{\omega_d}. \tag{21}$$

Satisfying the constraint in (21) will therefore guarantee the existence of a $g_2(j\omega_d)$, which can meet both constraints of (19) and (20), for plant i and column c. Given that the plant is 2×2, there will be two concentric "stay-in" discs at the origin, and two concentric "stay-out" discs, centered at $-1/p^i_{22}(j\omega_d)$ (one set from each row of (16)). A necessary condition for the existence of a $g_2(j\omega_d)$, which satisfies the four constraints in (16) for every plant instance, is generalized as

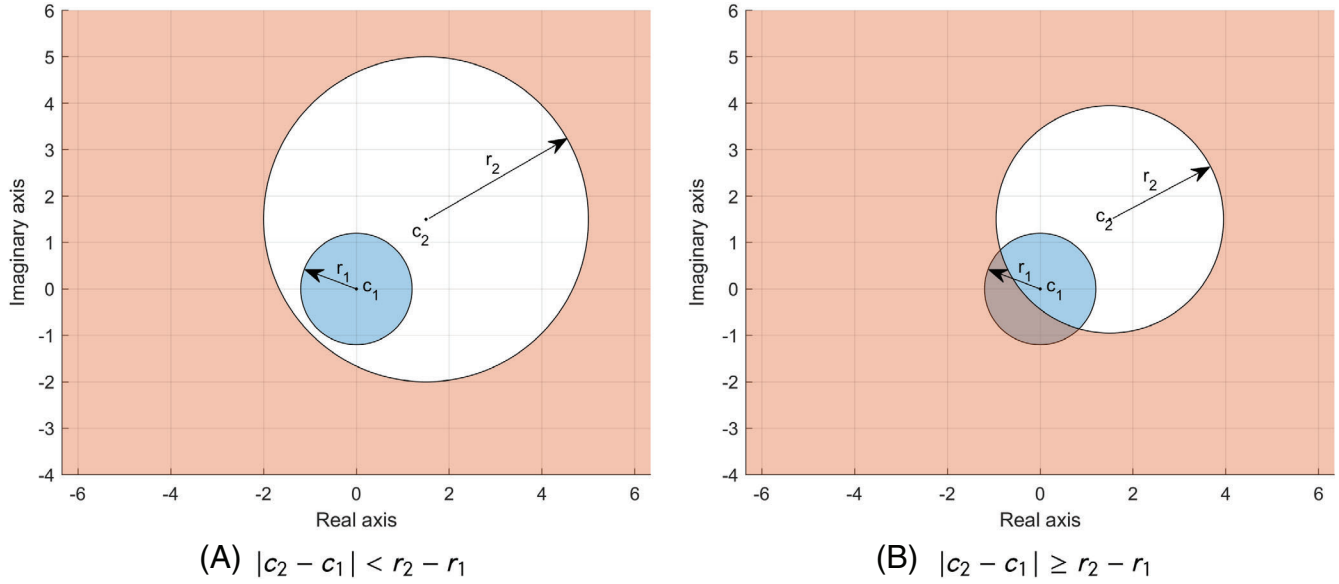

FIGURE 4 Arithmetic-complex plane showing an example of the admissible design regions (shaded) of $g_2(j\omega_d)$: "stay-in" disc (blue) and "stay-out" disc (white). A, An empty (invalid) design region when the "stay-out" disc envelops the "stay-in" disc. B, A nonempty design region when the "stay-out" disc does not fully envelop the "stay-in" disc [Colour figure can be viewed at wileyonlinelibrary.com]

$$\left|\frac{1}{p_{22}}\right|_{\omega_d}^{i} \geq \frac{|k_{2q}| + \beta_{1r}|p_{21}||g_1|}{\beta_{2q}|p_{22}|}\Bigg|_{\omega_d}^{i} - \frac{\beta_{1r}|1 + p_{11}g_1| - |k_{1r}|}{\beta_{2q}|p_{12}|}\Bigg|_{\omega_d}^{k}, \quad \forall q, r \in \{1, 2\}, \quad \forall i, k \in \{1, 2, \dots, n\}. \tag{22}$$

Additionally, the generalized constraint on $g_1(j\omega_d)$ to ensure that the radii of the "stay-in" discs in (19) are positive, is

$$|1 + p_{11}g_1|_{\omega_d}^{i} \geq \frac{|k_{1r}|}{\beta_{1r}}\Bigg|_{\omega_d}^{k} i, \quad \forall r \in \{1, 2\}, \quad \forall i \in \{1, 2, \dots, n\}. \tag{23}$$

Note that if, at a particular phase angle of $g_1(j\omega_d)$, the radius of the "stay-in" disc is always greater than or equal to the radius of the "stay-out" disc ($r_1 \geq r_2,\ \forall|g_1(j\omega)|$), any value of $|g_1(j\omega_d)|$ will guarantee the existence of $g_2(j\omega_d)$, for the particular plant instance. By extension, if the radius of the smallest "stay-in" disc (across the enumerated plant set) is always greater than or equal to the radius of the largest "stay-out" disc (at a particular phase angle of $g_1(j\omega_d)$), any selection of $|g_1(j\omega_d)|$ will guarantee the existence of $g_2(j\omega_d)$, for the entire plant set. In other words, at certain phase angles of $g_1(j\omega)$, (22) may become a sufficient condition for the existence of a globally valid $g_2(j\omega)$ that satisfies (16). Equations (22) and (23) are applied to the enumerated plant set, $P^i(j\omega_d) \in \mathcal{P}(j\omega_d)$, at design frequency point ω_d, and the intersection of all resulting design regions will describe the global solution space of $g_1(j\omega_d)$, for the particular non-plant-inverting splitting, namely $\mathbb{S}^P_{g_1(j\omega_d)}$. This solution space is expected to allow lower gain design in the mid to high frequencies, to the extent permitted by stability constraints.

3.1.3 | Finding the design regions on $g_r(j\omega_d)$

Equations (11), (22), and (23) indirectly describe the constraints on the first controller to be designed (eg, $g_1(s)$). In order to find the explicit constraints on the feedback controller element in question, one can fix the phase of $g_1(s)$ as $\phi_1 \in [-\pi, \pi]$, and then use the method of repeatedly squaring and rearranging, until one arrives at a polynomial inequality in $|g_1(j\omega_d)|$.[13] Explicitly, (11), (22), and (23) can be written generically at equality as

$$\gamma = |z_1(g_1)| + \lambda|z_2(g_1)|, \tag{24}$$

where γ and λ are constants, and $z_k(g_1) = z_k(|g_1|e^{j\phi_1})$ is a complex number, which behaves linearly with respect to $g_1(j\omega_d)$. Given that the magnitude of a complex number is $|z_k| = \sqrt{z_k z_k^*}$, we aim to arrive at an equation which contains only even powers of all z_k terms, which will correspond to a polynomial in $|g_1(j\omega_d)|$. Squaring both sides of (24) and rearranging yields

$$\gamma^2 - |z_1(g_1)|^2 - \lambda^2|z_2(g_1)|^2 = 2\lambda|z_1(g_1)||z_2(g_1)|. \tag{25}$$

Squaring once more generates the desired result of

$$(\gamma^2 - |z_1(g_1)|^2 - \lambda^2|z_2(g_1)|^2)^2 = 4\lambda^2|z_1(g_1)|^2|z_2(g_1)|^2. \tag{26}$$

The possible phase angles of $g_1(j\omega_d)$ can be swept through, across the allowable range of $[-\pi, \pi]$, thereby making (26) solely a function of $|g_1(j\omega_d)|$. As $z_k(g_1)$ is linear with respect to $g_1(j\omega_d)$, (26) will (after some rearranging) describe the quartic polynomial,

$$|g_1(j\omega_d)|^4 + a_1|g_1(j\omega_d)|^3 + a_2|g_1(j\omega_d)|^2 + a_3|g_1(j\omega_d)| + a_4 = 0, \tag{27}$$

where the coefficients in (27) are made up of elements of $P^i(j\omega_d)$, $P^k(j\omega_d)$, $\hat{P}^i(j\omega_d)$, $\hat{P}^k(j\omega_d)$, $M(j\omega_d)$, $\beta(\omega_d)$, and ϕ_1 (depending on the particular splitting). The roots of the quartic polynomial will correspond to the design boundaries on $|g_1(j\omega_d)|$, for the particular controller phase ϕ_1 and plant (or plant pairing). As the squaring process may yield roots which do not correspond to the original inequality (each squaring may double the number of roots with some of these being invalid), these roots need to be checked against the original inequality. To determine whether the boundaries are "stay-above" or "stay-below," one may need to evaluate the original inequality at a value of $|g_r(j\omega_d)|$ between two valid roots. If the result satisfies the inequality, the design region between the two roots is "stay-in," implying the adjacent regions are "stay-out," and vice versa.

3.1.4 | Union of design regions

As the solution spaces from both the plant-inverting and non-plant-inverting methods overbound the viable design region of $g_1(j\omega_d)$, the union of the two individual solution spaces,

$$\mathbb{S}_{g_1(j\omega_d)} = \mathbb{S}^{\hat{P}}_{g_1(j\omega_d)} \cup \mathbb{S}^{P}_{g_1(j\omega_d)}, \tag{28}$$

can only enlarge the attainable design region of $g_1(j\omega_d)$. Applying the union operation at all discrete design frequency points also has the potential benefit of expanding the design regions at the midfrequencies (relative to current plant-inverting methods). This is especially important for efficient design in the gain-phase crossover region. The global solution space of (28) can be visualized in the log-polar plane and used to design a $g_1(s)$, which satisfies all the discrete tracking requirements,

$$g_1(j\omega_d) \in \mathbb{S}_{g_1(j\omega_d)}, \quad \forall \omega_d \in \Omega. \tag{29}$$

It must be stressed that the existence of a nonempty $\mathbb{S}_{g_1(j\omega_d)}$, $\forall \omega_d \in \Omega$, does not guarantee that a low-order, proper, rational, causal $g_1(s)$ can be designed which simultaneously meets all the discrete design frequency requirements (ie, joining the dots may not be possible/feasible!).

3.1.5 | Closure of the second feedback loop

With the first loop closed (eg, $g_1(s)$), the design of $g_2(s)$ can proceed. Again, using the constraint in (11), one can arrive at a global solution space for $g_2(j\omega_d)$, for the particular plant-inverting splitting, namely, $\mathbb{S}^{\hat{P}}_{g_2(j\omega_d)}$. Note that this is a non-sequential approach, which does not take into account the selection of $g_1(s)$. Given that the non-plant-inverting method

is sequential, the order in which the controller elements are designed does affect the overall system performance. The preferred order depends on (i) the closed-loop bandwidth of each loop, (ii) the elementwise uncertainty, (iii) channel interactions, and (iv) the underlying tracking specifications. As such, the designer must exercise engineering understanding of the problem to select the design order for the particular problem. The full design region on $g_2(j\omega_d)$ follows as the union of the two individual regions,

$$\mathbb{S}_{g_2(j\omega_d)} = \mathbb{S}^{\hat{P}}_{g_2(j\omega_d)} \cup \mathbb{S}^{P}_{g_2(j\omega_d)}, \tag{30}$$

and successful design of $g_2(s)$ is necessitated by

$$g_2(j\omega_d) \in \mathbb{S}_{g_2(j\omega_d)}, \quad \forall \omega_d \in \Omega, \tag{31}$$

assuming $g_2(s)$ is feasible and physically implementable.

3.2 | Feedforward controller design

Once $G(s)$ has been designed, $X(s)$ can be designed in earnest. To assess the effect of $X(j\omega_d)$ on $E(j\omega_d)$, the discretized matrix error equation in (2) can be written explicitly as

$$E^i(j\omega_d) = (I + PG)^{-1}(M - PX)|^i_{\omega_d} = \begin{bmatrix} a_1 + a_2x_{11} + a_3x_{21} & b_1 + b_2x_{12} + b_3x_{22} \\ c_1 + c_2x_{11} + c_3x_{21} & d_1 + d_2x_{12} + d_3x_{22} \end{bmatrix}^i_{\omega_d}, \tag{32}$$

where the coefficients in (32) are constant complex numbers, made up of elements from $P^i(j\omega_d)$, $M(j\omega_d)$, and $G(j\omega_d)$. Notably, $x_{11}(j\omega_d)$ and $x_{21}(j\omega_d)$ only affect the first column of (32), whereas $x_{12}(j\omega_d)$ and $x_{22}(j\omega_d)$ only affect the second column. Applying the original tracking specification of (3) to the first column of (32) gives the two constraints of

$$\begin{bmatrix} |a_1 + a_2x_{11} + a_3x_{21}| \\ |c_1 + c_2x_{11} + c_3x_{21}| \end{bmatrix}^i_{\omega_d} \preceq \begin{bmatrix} \beta_{11}(\omega_d) \\ \beta_{21}(\omega_d) \end{bmatrix}. \tag{33}$$

Next, dividing the first row of (33) by $|a^i_3(j\omega_d)|$ and the second row by $|c^i_3(j\omega_d)|$ gives

$$\begin{bmatrix} |(a_1 + a_2x_{11})/a_3 + x_{21}| \\ |(c_1 + c_2x_{11})/c_3 + x_{21}| \end{bmatrix}^i_{\omega_d} \preceq \begin{bmatrix} \beta_{11}/|a_3| \\ \beta_{21}/|c_3| \end{bmatrix}^i_{\omega_d}. \tag{34}$$

The admissible design regions of $x_{21}(j\omega_d)$ in (34), with respect to the constraints on plant i, are two "stay-in" discs, where the two centers are at $-(a_1 + a_2x_{11})/a_3|^i_{\omega_d}$ and $-(c_1 + c_2x_{11})/c_3|^i_{\omega_d}$, and the corresponding radii are $\beta_{11}(\omega_d)/|a^i_3(j\omega_d)|$ and $\beta_{21}(\omega_d)/|c^i_3(j\omega_d)|$, respectively. Simultaneously satisfying both constraints requires a nonempty intersection of the two "stay-in" discs. As in the case of (11) and Figure 3, this requires that the distance between the two centers must be smaller than or equal to the sum of the respective radii,

$$|(a_1 + a_2x_{11})/a_3 - (c_1 + c_2x_{11})/c_3|^i_{\omega_d} \leq \beta_{11}(\omega_d)/|a^i_3(j\omega_d)| + \beta_{21}(\omega_d)/|c^i_3(j\omega_d)|. \tag{35}$$

Satisfying the inequality in (35) will guarantee the existence of a nonempty solution space for $x_{21}(j\omega_d)$, which can achieve (34) for plant instance i. Given that plant pair $\{i,k\}$ will collectively generate four discoidal solution spaces on $x_{21}(j\omega_d)$, based on (34), the set of necessary conditions for the existence of a common $x_{21}(j\omega_d)$, which can simultaneously satisfy all four design regions, is

$$|(a^i_1 + a^i_2x_{11})/a^i_3 - (c^k_1 + c^k_2x_{11})/c^k_3|_{\omega_d} \leq \beta_{11}(\omega_d)/|a^i_3(j\omega_d)| + \beta_{21}(\omega_d)/|c^k_3(j\omega_d)|, \tag{36}$$

$$|(a_1^i + a_2^i x_{11})/a_3^i - (a_1^k + a_2^k x_{11})/a_3^k|_{\omega_d} \leq \beta_{11}(\omega_d)(1/|a_3^i(j\omega_d)| + 1/|a_3^k(j\omega_d)|), \tag{37}$$

$$|(c_1^i + c_2^i x_{11})/c_3^i - (c_1^k + c_2^k x_{11})/c_3^k|_{\omega_d} \leq \beta_{21}(\omega_d)(1/|c_3^i(j\omega_d)| + 1/|c_3^k(j\omega_d)|). \tag{38}$$

Equations (36), (37), and (38) describe a set of discoidal "stay-in" design regions on $x_{11}(j\omega_d)$ for plant pair $\{i, k\}$. Applying (36), (37), and (38) to the enumerated plant set ($\{i, k\} \in \{1,2, \dots, n\}$), and then taking the intersection of the resulting design regions, describes the global solution space of $x_{11}(j\omega_d)$, namely, $\mathbb{S}_{x_{11}(j\omega_d)}$. Visualization of $\mathbb{S}_{x_{11}(j\omega_d)}$ and design of $x_{11}(s)$ can take place in the log-polar plane, and upon finding an $x_{11}(s)$ which satisfies (36), (37), and (38), for every ordered plant pair, the corresponding discretized design regions of $x_{21}(s)$ will form in the arithmetic-complex plane, based on (34) (if it exists). Similarly, the necessary set of constraints on $x_{12}(j\omega_d)$ governing the existence of an $x_{22}(j\omega_d)$ that satisfies the tracking requirements of plant pair $\{i,k\}$, is

$$|(b_1^i + b_2^i x_{12})/b_3^i - (d_1^k + d_2^k x_{12})/d_3^k|_{\omega_d} \leq \beta_{12}(\omega_d)/|b_3^i(j\omega_d)| + \beta_{22}(\omega_d)/|d_3^k(j\omega_d)|. \tag{39}$$

$$|(b_1^i + b_2^i x_{12})/b_3^i - (b_1^k + b_2^k x_{12})/b_3^k|_{\omega_d} \leq \beta_{11}(\omega_d)(1/|b_3^i(j\omega_d)| + 1/|b_3^k(j\omega_d)|), \tag{40}$$

$$|(d_1^i + d_2^i x_{12})/d_3^i - (d_1^k + d_2^k x_{12})/d_3^k|_{\omega_d} \leq \beta_{21}(\omega_d)(1/|d_3^i(j\omega_d)| + 1/|d_3^k(j\omega_d)|). \tag{41}$$

The design of $x_{11}(s)$ and $x_{12}(s)$ takes place independently, and upon adhering to the aforementioned constraints, allows for the subsequent design of $x_{21}(s)$ and $x_{22}(s)$ (if the corresponding solution space is nonempty). It is worth emphasizing that the resulting design regions on $x_{rc}(j\omega_d)$ do not possess any design conservatism as a result of overbounding. As in the case of designing $G(s)$, it may not be feasible/possible to find a $X(s)$, which can simultaneously meet all the discrete design specifications, as $X(s)$ must obey the Bode gain-phase constraints. Note that by dividing the first row of (33) by $|a_2^i(j\omega_d)|$ and the second row by $|c_2^i(j\omega_d)|$, one can arrive at constraints on $x_{21}(j\omega_d)$, instead of $x_{11}(j\omega_d)$. In other words, the designer can choose the order in which the elements of $X(s)$ are designed. As in the sequential non-plant-inverting design methodology of $G(s)$, the design order of $X(s)$ must be selected by the designer, based on engineering understanding of the problem.

Section 3.2 describes how bounds on $x_{rc}(s)$ are obtained sequentially. Because $X(s)$ in Figure 2 is not part of the feedback structure, if preview of $r(t)$ is available (eg, following a known trajectory), in principle $X(s)$ does not need to be a causal function. One might then instead design the signal $v(s) = X(s)r(s)$ directly. This will not be provided in detail here.

4 | WORKED EXAMPLE

In order to demonstrate the efficacy of the proposed method, we apply our design routine to a simple problem,[14] with an existing (recently published) solution.[10] The uncertain plant is

$$\mathbf{P}(s) = \frac{1}{s}\begin{bmatrix} k_{11} & k_{12} \\ k_{21} & k_{22} \end{bmatrix}, \quad \{k_{11}, k_{22}\} \in [2, 6], \quad \{k_{12}, k_{21}\} \in [0.5, 1.5]. \tag{42}$$

The corresponding reference model and tracking error bounds, in the frequency band of $\omega \leq 10$ rad/s, are given as

$$M(s) = \text{diag}\left\{\frac{1}{1 + s/3}, \frac{1}{1 + s/3}\right\}, \quad \beta_{rc}(\omega) = 0.2\omega\sqrt{1 + \omega^2/9}. \tag{43}$$

Additionally, the high frequency sensitivity constraint ($\omega \geq 10$ rad/s) is

$$\left.\frac{1}{|1 + g_{rr}/\hat{p}_{rr}|}\right|_{\omega_d}^{i} \leq 1.67, \quad \forall i = \{1, 2, \dots, N\}. \tag{44}$$

TABLE 1 Optimized selection of $X(j\omega_d)$ for non-plant-inverting method, evaluated at $\omega_d \in \{1, 2, 3, 5, 8, 10\}$ rad/s, over 256 plant cases

ω_d	1	2	3	5	8	10
$x_{11}(j\omega_d), x_{22}(j\omega_d)$	0.0800 + 0.2400i	0.2049 + 0.3074i	0.3388 + 0.3389i	0.5882 + 0.3529i	0.7013 + 0.2630i	0.6023 + 0.1807i
$x_{12}(j\omega_d), x_{21}(j\omega_d)$	−0.0142 − 0.0426i	−0.0615 − 0.0923i	−0.1000 − 0.1000i	−0.0947 − 0.0568i	−0.1135 − 0.0426i	−0.1171 − 0.0351i

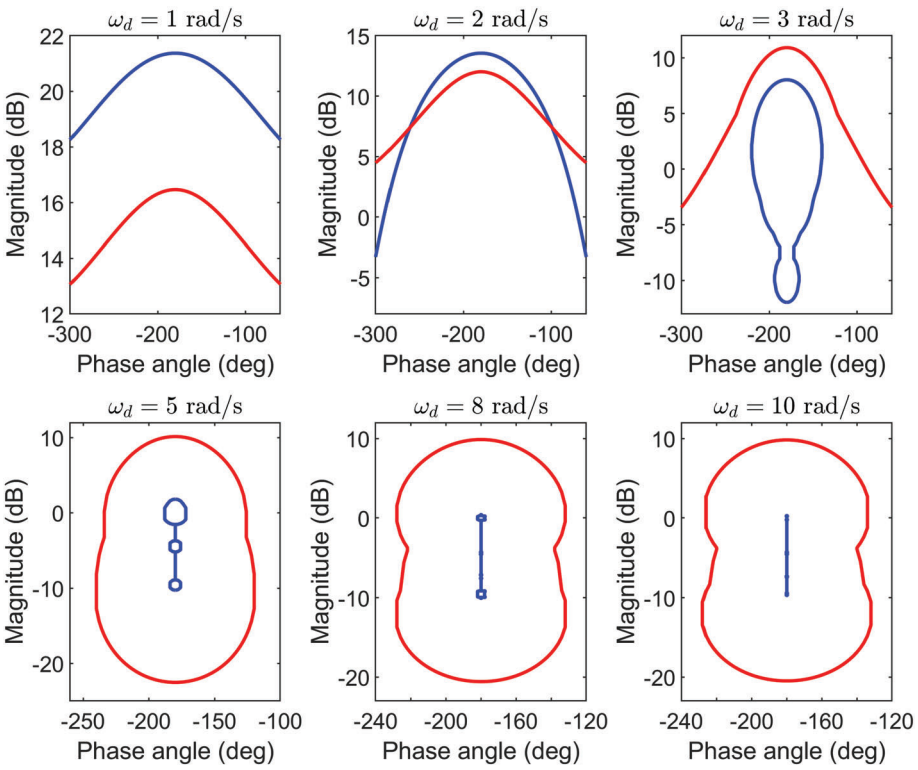

FIGURE 5 Log-polar plot showing per-frequency "stay-out" tracking design regions resulting from the plant-inverting method (red), and non-plant-inverting method (blue), for $l^0_{11}(j\omega)$, and $\Omega = \{1, 2, 3, 5, 8, 10\}$ rad/s [Colour figure can be viewed at wileyonlinelibrary.com]

The plant-inverting design methods in References 10,14 resulted in highly conservative mid- to high-frequency constraints on the feedback controllers, meaning that a universal sensitivity constraint was never required (low sensitivity was implicitly enforced by the conservative tracking boundaries at the chosen design frequencies). As the proposed non-plant-inverting design routine is expected to yield less conservative design regions on the feedback controller at the mid to high frequencies, the sensitivity specification from (44) is adjusted to cover the entire frequency spectrum. With reference to Section 3.1, two sets of design regions on the first feedback controller ($g_1(s)$ in this case) are generated. In the case of the non-plant-inverting method, the optimized frequency response of $X(j\omega_d)$, at each discrete design frequency point, is shown in Table 1. Note that the symmetry of the plant and specifications set results in a symmetrical $X(j\omega_d)$ at each discrete design frequency point.

Figure 5 shows the resulting tracking design regions, by individually applying the aforementioned methods, on (arbitrarily selected) nominal loop transfer $l^0_{11}(s) = p^0_{11}(s)g(s)$, for 256 plant cases, where $p^0_{11}(s) = 2/s$.

Note that the choice of nominal plant $p^0_{11}(s)$ has no effect on the design region of $g_1(s)$, and is only required for producing the traditional Nichols Chart visualization. As expected, the plant-inverting method produces lower gain requirements on $g_1(s)$ at low frequencies, whereas the non-plant-inverting method performs better at higher frequencies (including the gain-phase crossover region). In fact, the "stay-out" regions at $\omega_d \geq 8$ rad/s, from the non-plant-inverting method, are barely visible (as a result of the ease of meeting the large high frequency tracking tolerance specified). The union of the design regions in Figure 5 will then describe the expanded design region of the proposed complementary design method. Figure 6 compares this resulting design region with the method in Reference 10.

The design boundaries of the proposed method at $\omega_d = 1$ rad/s are similar to that of Reference 10, but the significant boundary differences can be seen at the higher frequencies, that is, at and above the gain crossover frequency, where the conservatism can be most problematic. With reference to (23), the "stay-out" region on $g_1(j\omega_d)$ will approach the set of

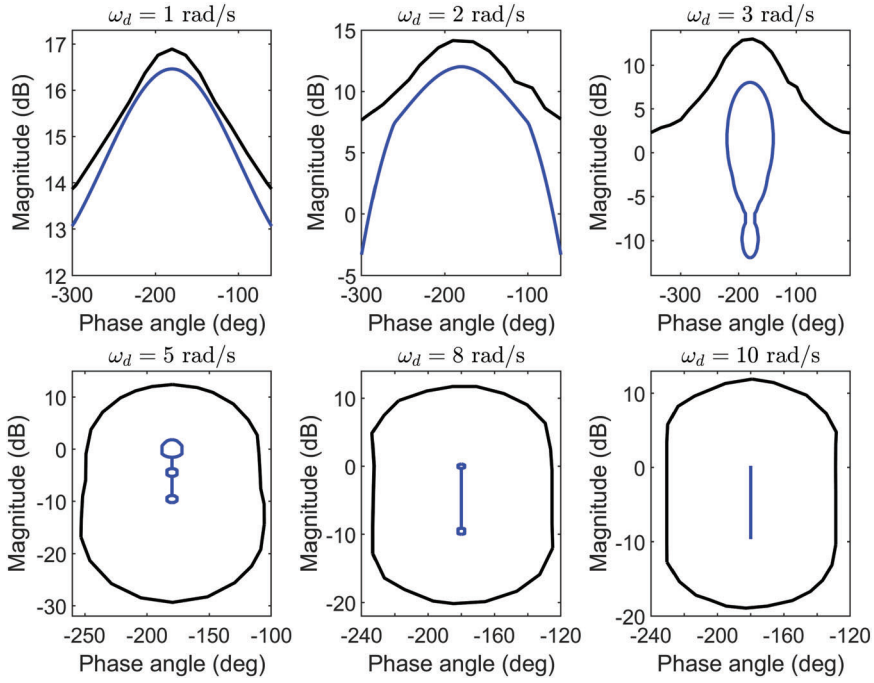

FIGURE 6 Log-polar plot showing per-frequency "stay-out" tracking design regions resulting from proposed complementary design method (blue), and method detailed in Reference 10 (black), for $l_{11}^0(j\omega)$, and $\Omega = \{1, 2, 3, 5, 8, 10\}$ rad/s [Colour figure can be viewed at wileyonlinelibrary.com]

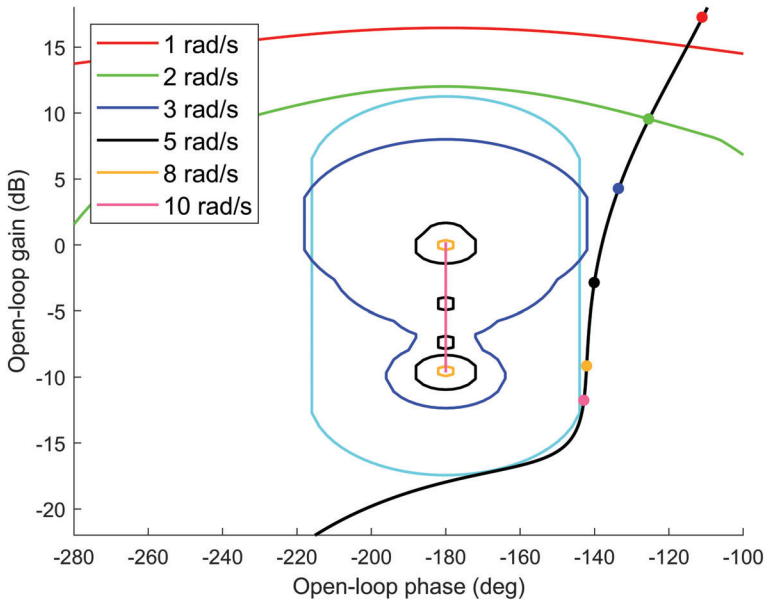

FIGURE 7 Log-polar plot showing the union of "stay-out" tracking bounds for discrete design frequency range $\Omega = \{1, 2, 3, 5, 8, 10\}$ rad/s, as well as universal "stay-out" sensitivity bound (cyan), on $l_{11}^0(s)$. The designed $l_{11}^0(s)$ is also shown [Colour figure can be viewed at wileyonlinelibrary.com]

plant dependent critical points, for sufficiently high frequencies, which can be seen as a vertical line in Figures 5 and 6 (in stark contrast to the high frequency design regions resulting from plant-inverting methods). As is evident from the lower gain requirements in Figure 6, the proposed method outperforms the method in Reference 10 at all design frequencies and feedback controller phase angles.

The resulting union of tracking boundaries on $g_1(s)$, as well as the adjusted sensitivity requirements from (44) are shown in Figure 7.

A viable $g_1(s)$, which meets all the design requirements, is also shown in Figure 7 (after shifting and scaling by $p_{11}^0(s) = 2/s$), and is described by

$$g_1(s) = \frac{4\left(1 + \frac{s}{11.26}\right)}{\left(1 + \frac{s}{2.173}\right)\left(1 + 2\frac{0.32s}{25.20} + \frac{s^2}{25.20^2}\right)}. \tag{45}$$

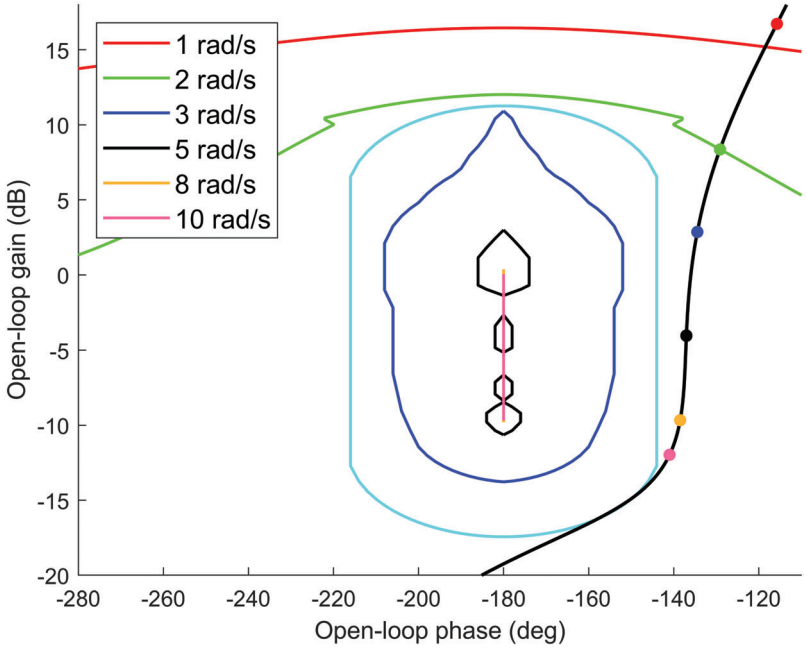

FIGURE 8 Log-polar plot showing the union of "stay-out" tracking bounds for discrete design frequency range $\Omega = \{1, 2, 3, 5, 8, 10\}$ rad/s, as well as universal "stay-out" sensitivity bound (cyan), on $l^0_{22}(s)$. The designed $l^0_{22}(s)$ is also shown [Colour figure can be viewed at wileyonlinelibrary.com]

With reference to Figure 7, the universal sensitivity bound dominates the tracking bounds for $\omega > 3$ rad/s, resulting in overdesign in the mid to high frequencies (as a result of the poor compatibility between the tracking and sensitivity specifications). Overdesign at $\omega_d = 1$ rad/s is required to accommodate the low-frequency tracking requirements for $\omega \leq 0.1$ rad/s (not shown in Figure 7).

Following the successful design of $g_1(s)$, the design of $g_2(s)$ proceeds. Figure 8 shows the union of tracking bounds as well as the sensitivity constraint for $g_2(s)$. The designed $g_2(s)$ is also shown in Figure 8 (after shifting and scaling by $p^0_{22}(s) = 2/s$), and is described by

$$g_2(s) = \frac{4\left(1 + \frac{s}{6.48}\right)}{\left(1 + \frac{s}{1.59}\right)\left(1 + 2\frac{0.49s}{23.41} + \frac{s^2}{23.41^2}\right)}. \tag{46}$$

As in the case of Figure 7, the tracking bounds in Figure 8 are dominated by the sensitivity constraint for $\omega \geq 3$ rad/s, resulting in overdesign in the gain-phase crossover region ($g_2(s)$ has to roll off later to accommodate the universal sensitivity constraint).

With the feedback design complete, the last step is to design the feedforward filter $X(s)$. With reference to Section 3.2, one can choose the order in which the elements of $X(s)$ are to be designed. The diagonal elements of $X(s)$ are designed first, after which the off-diagonal terms can be designed. The resulting design boundaries on $X(s)$ are shown in Figure 9. Given the control structure in Figure 2, a subtle condition on $X(s)$ to achieve zero-error tracking at steady state is for $X(s)$ to have zero DC gain (requiring derivative action). This is analogous to $F(s)$ requiring unitary DC gain in Figure 1. An appropriate $X(s)$, which meets all the design constraints, is

$$X(s) = \begin{bmatrix} \frac{9.36s}{(1+s/1.70)(1+s/8.19)} & \frac{-6.74s}{(1+s/3.76)(1+s/5.32)} \\ \frac{-5.85s}{(1+s/1.77)(1+s/7.68)} & \frac{7.52s}{(1+s/1.70)(1+s/8.19)} \end{bmatrix}, \tag{47}$$

and is also shown in Figure 9. The ease of meeting the per-frequency design boundaries in Figure 9 (especially at the mid to high frequencies) is attributed to the overdesign of the feedback controller, resulting from the dominant sensitivity specifications in Figures 7 and 8. Successful design of $G(s)$ and $X(s)$ is validated by plotting the magnitude of the set of closed-loop error frequency responses against the error tolerances from (43), as shown in Figure 10. It is worth pointing out that the designed feedback controllers in (45) and (46) are of the same order as that of the feedback solution in Reference 10, and possess equivalent or lower gain at all frequencies. With reference to Figure 10, the amount of overdesign is most

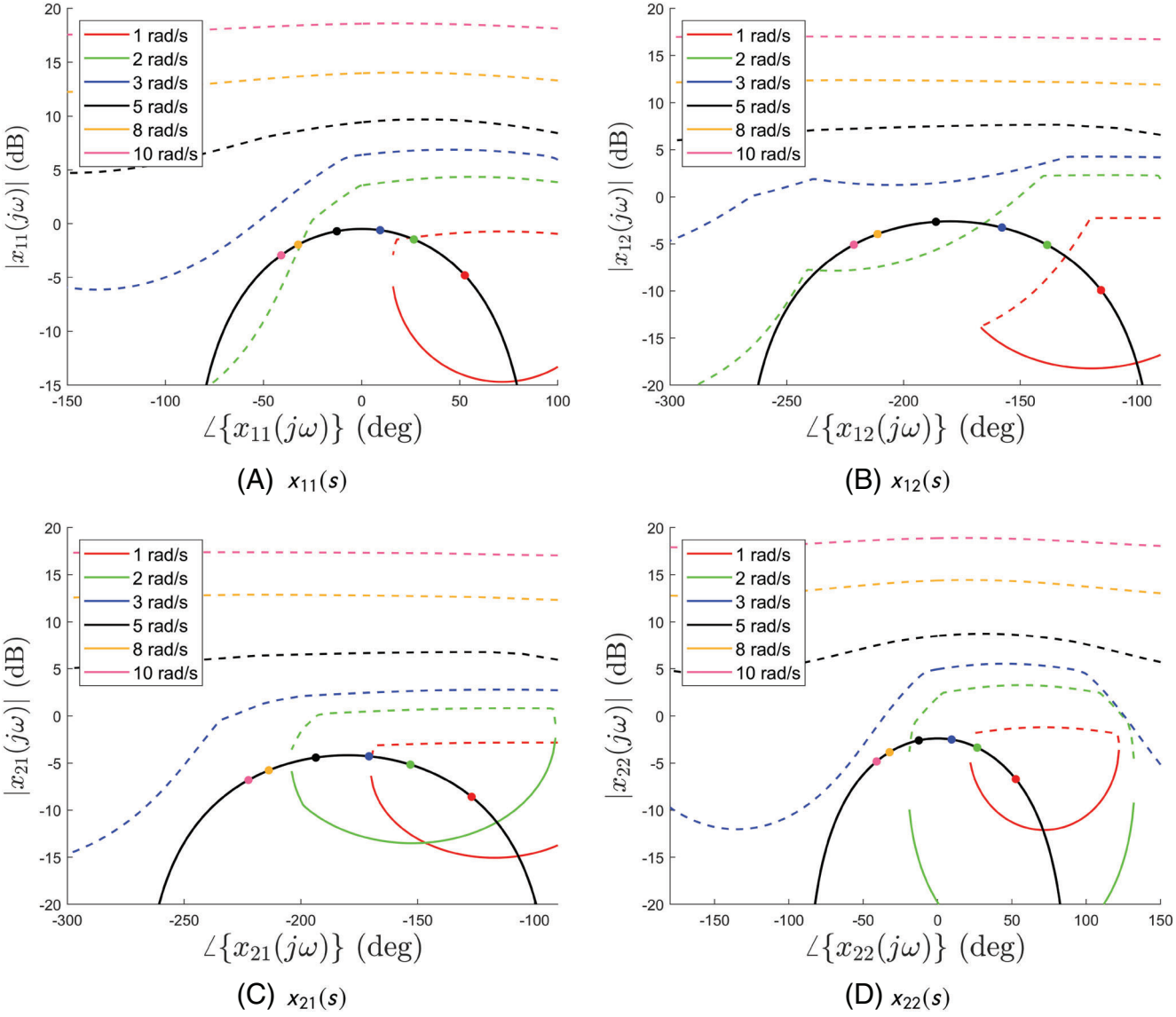

FIGURE 9 Log-polar plane showing design boundaries on $X(s)$, for discrete design frequency set $\Omega = \{1, 2, 3, 5, 8, 10\}$ rad/s. Solid lines indicate "stay-above" bounds, whereas dashed lines indicate "stay-below" bounds. The designed feedforward controllers for the respective design conditions are also shown [Colour figure can be viewed at wileyonlinelibrary.com]

noticeable at the mid to high frequencies, as a result of the sensitivity requirements dominating the tracking requirements in that frequency band. The compatibility between the enumerated plant set and the prescribed tracking specifications will also naturally affect the amount of potential overdesign at each design frequency.[15] This is analogous to the poor compatibility between the sensitivity and tracking bounds (the large tracking error tolerances were easy to achieve in the gain-phase crossover region using the non-plant-inverting design method, which was previously not possible using plant-inverting methods).

5 | CONCLUSION

This article has presented a complementary QFT design method, intended for 2×2 systems, which is capable of reducing feedback control overdesign across the entire frequency range of interest. In particular, the combination of a plant-inverting and non-plant-inverting bound generation routine reduces the conservatism at the gain-phase crossover

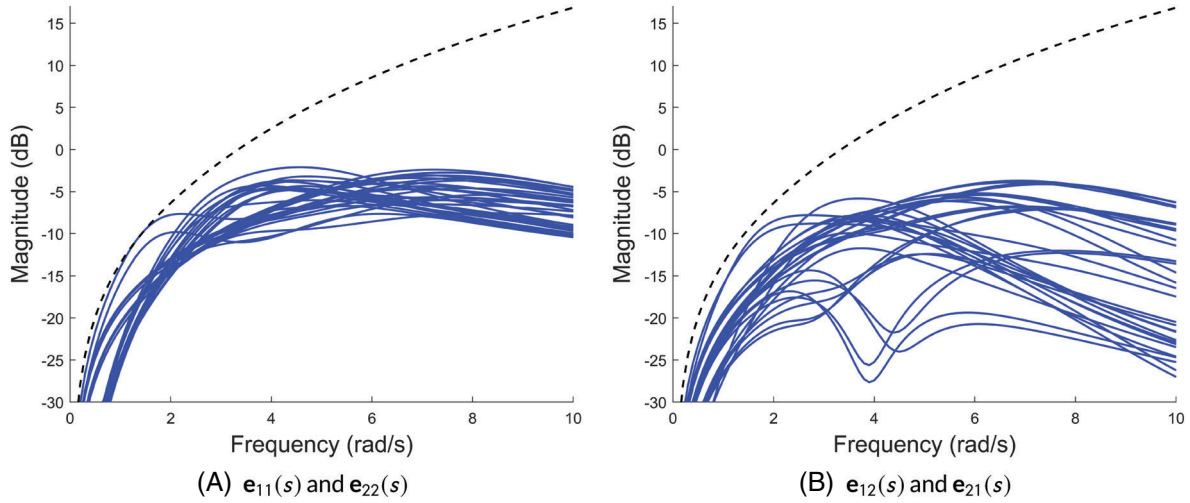

FIGURE 10 Bode magnitude plots comparing closed-loop error tracking behavior (solid blue lines) with adjusted error tolerances (dashed black line). A, Diagonal tracking behavior. B, Nondiagonal tracking behavior[Colour figure can be viewed at wileyonlinelibrary.com]

region, allowing for more efficient feedback control design. Following the successful feedback controller design, a nondiagonal feedforward filter was designed, without requiring overbounding approximations. This method has been applied to a simple, but suitably coupled 2×2 system, and was shown to outperform preexisting methods, especially at higher frequencies of interest.

ACKNOWLEDGEMENT

This work was supported by the South African National Research Foundation, Grant Number: 81148.

ORCID

Arnold Pretorius https://orcid.org/0000-0002-1940-588X
Edward Boje https://orcid.org/0000-0003-2733-3537

REFERENCES

1. Horowitz IM. *Synthesis of Feedback Systems*. Elsevier; 2013. https://books.google.co.za/books?hl=en&lr=&id=qykSBQAAQBAJ&oi=fnd&pg=PP1&dq=synthesis+of+feedback+systems&ots=okdQj-rwhj&sig=84MkSM21sS4bStGqaogDOL2chaY#v=onepage&q=synthesis%20of%20feedback%20systems&f=false.
2. Elso J, Gil-Martinez M, Garcia-Sanz M. Nonconservative QFT bounds for tracking error specifications. *Int J Robust Nonlinear Control*. 2012;22(18):2014-2025.
3. Elso J, Gil-Martinez M, Garcia-Sanz M. Quantitative feedback–feedforward control for model matching and disturbance rejection. *IET Control Theory Appl*. 2013;7(6):894-900.
4. Horowitz I. Survey of quantitative feedback theory (QFT). *Int J Robust Nonlinear Control IFAC-Affiliat J*. 2001;11(10):887-921.
5. Horowitz I. Quantitative synthesis of uncertain multiple input-output feedback system. *Int J Control*. 1979;30(1):81-106.
6. Bailey F, Hui CH. Cacsd tools for loop gain-phase shaping design of SISO robust controllers. Paper presented at: Proceedings of the IEEE Control Systems Society Workshop on Computer-Aided Control System Design; 1989:151-157; IEEE.
7. Eitelberg E. Quantitative feedback design for tracking error tolerance. *Automatica*. 2000;36(2):319-326.
8. Boje E. Multivariable quantitative feedback design for tracking error specifications. *Automatica*. 2002;38(1):131-138.
9. Alavi SM, Khaki-Sedigh A, Labibi B, Hayes M. Improved multivariable quantitative feedback design for tracking error specifications. *IET Control Theory Appl*. 2007;1(4):1046-1053.
10. Elso J, Gil-Martinez M, Garcia-Sanz M. A quantitative feedback solution to the multivariable tracking error problem. *Int J Robust Nonlinear Control*. 2014;24(16):2331-2346.
11. Elso J, Gil-Martinez M, Garcia-Sanz M. Quantitative feedback control for multivariable model matching and disturbance rejection. *Int J Robust Nonlinear Control*. 2017;27(1):121-134.
12. Garcia-Sanz M. *Robust Control Engineering: Practical QFT Solutions*. CRC Press; 2017. https://books.google.co.za/books?hl=en&lr=&id=HgsqDwAAQBAJ&oi=fnd&pg=PP1&dq=robust+control+engineering+practical+qft&ots=mQSdzFRqgH&sig=ZsFAdjA2ALWCmHG6Us-NLh9cfE4#v=onepage&q=robust%20control%20engineering%20practical%20qft&f=false.
13. Boje E. Algorithm for calculating mimo qft tracking bounds. *J Dyn Syst Measur Control*. 2004;126(3):697-699.

14. Yaniv O, Chait Y. A simplified multi-input multi-output formulation for the quantitative feedback theory; 1992.
15. Pretorius A, Boje E. Robust plant by plant control design using model-error tracking sets. *Int J Robust Nonlinear Control*. 2019;29:3330-3340.

SUPPORTING INFORMATION

Additional supporting information may be found online in the Supporting Information section at the end of this article.

How to cite this article: Pretorius A, Boje E. A complementary quantitative feedback theory solution to the 2×2 tracking error problem. *Int J Robust Nonlinear Control*. 2020;30:6569–6584. https://doi.org/10.1002/rnc.5120